Submitted to the International Europhysics Conference on High Energy Physics,
HEP97, Jerusalem, Israel, August 1997

Elastic Electroproduction of ϱ and ϕ Mesons for $1 < Q^2 < 5$ GeV^2 at HERA

H1 Collaboration

Abstract

A measurement of the cross–section for the elastic electroproduction of ϱ and ϕ mesons is presented for the photon virtuality in the range $1 < Q^2 < 5$ GeV^2 and for the hadronic centre of mass energy in the range $40 < W < 140$ GeV. The analysed data were taken in 1995 with special HERA operating conditions in which the interaction vertex was shifted by 70 cm into the direction of the outgoing proton. The shape of the ϱ mass distribution is studied as a function of Q^2. Measurements are presented of the dependences of the ϱ and ϕ cross–sections on Q^2, on t (the four–momentum tranfer to the proton), and of the vector meson polarisation state. The ratio of the elastic production cross–sections for ϕ and ϱ mesons is determined.

Abstract 381
Parallel Sessions 2,3,4
Plenary Sessions 1,2,3

1 Introduction

The subject of this paper is the study by the H1 Collaboration of elastic ϱ and ϕ meson electroproduction for $1 < Q^2 < 5$ GeV^2 and $40 < W < 140$ GeV. Q^2 is minus the square of the exchanged photon four-momentum and W is the $\gamma^* p$ center of mass energy. The results are compared with ϱ and ϕ photoproduction data in fixed target, and in HERA [1] experiments. They are also compared with electro- and muoproduction at low W [2] and with electroproduction at HERA [3, 4, 5, 6].

After presentation of event selection and mass distributions, the total cross–sections and differential distributions are studied, in particular the energy dependence of the cross–section, the t distribution (t is the square of the four-momentum transfer from the photon to the target), the vector meson polarisation, and the evolution of the ϕ : ϱ cross–section ratio as a function of Q^2.

The data were collected in 1995 by the H1 experiment, when HERA operated with 820 GeV protons and 27.5 GeV positrons and with an interaction vertex position shifted by +70 cm with respect to the nominal position.[1] The data correspond to an integrated luminosity of 125 nb^{-1}. In the following we use the term vector meson production as a generically name for ϱ and ϕ meson production.

2 Event selection and kinematics

The processes under study are the elastic electroproduction of ϱ and ϕ mesons, analysed in their dominant decay modes into two charged hadrons (Fig. 1a):

$$e^+ + p \rightarrow e^+ + p + V, \qquad V = \varrho,\ \phi; \qquad \varrho \rightarrow \pi^+ + \pi^-, \qquad \phi \rightarrow K^+ + K^-. \tag{1}$$

The events selected in the H1 detector contain only a positron and two particles with opposite charges, originating from the interaction vertex.[2] The scattered proton remains in the beam pipe and is not detected due to the small momentum transfer to the target in diffractive interactions. The scattered positron is identified as an electromagnetic cluster of energy larger than 17 GeV detected in the H1 backward scintillating fibre calorimeter SpaCal [8], which is associated with a track segment in the backward drift chamber BDC situated in front of the SpaCal.

To ensure good trigger efficiency and good precision of the kinematic variable measurement, the extrapolation onto the SpaCal plane of the BDC track segment assigned to the positron must be recontructed outside a circle of 8.7 cm around the beam pipe, and the distance between that extrapolated point and the centre of gravity of the cluster in SpaCal must be less than 3 cm.

Two tracks of particles with opposite charges and transverse momentum larger than 100 MeV/c are required to be reconstructed in the H1 central tracking detector and to be linked to an interaction vertex with a z position in the interval +50 cm and +100 cm with respect to the nominal interaction point. The charge and momentum of the particles are measured thanks to the uniform 1.15 T magnetic field in the central part of the detector. No particle identification is required.

Backgrounds to reaction (1) are due to diffractive events in which the proton is excited into a system of higher mass, which subsequently dissociates (Fig. 1b), and from events in which the

[1] In the H1 coordinate system, the forward ($+z$) direction is that of the outgoing proton beam.
[2] A detailed description of the H1 detector can be found elsewhere [7].

photon is excited into a state subsequently decaying into two charged particles and additional neutral particles, notably the ω meson. The H1 detector allows an efficient reduction of these backgrounds to be made [3, 9]. No cluster (which is not associated with the decay particles of the vector meson) with energy greater the 0.5 GeV must be measured in the liquid argon calorimeter. No more than one hit pair must be detected in the first three layers of the forward muon system, and no hit must be registered in the proton remnant tagger situated at $z = +24$ m relative to the nominal interaction point.

The kinematic variables are the negative four-momentum squared of the photon Q^2, the total $\gamma^* p$ centre of mass energy W, and the square of the four-momentum transfer to the proton t. The variable Q^2 is reconstructed with the double angle method [10], using the polar angles of the scattered positron (measured from the BDC track segment and the interaction vertex) and of the vector meson candidate (obtained from the decay tracks). The variable W is reconstructed using the Jacquet-Blondel method [10], from the energy and the polar angle of the vector meson. The absolute value of t is very well approximated as the square of the transverse momentum of the outgoing proton. It is measured as the transverse momentum of the vector meson and the positron, where the energy of the positron is recalculated, assuming conservation of $\Sigma(E - p_z)$.[3]

To remove poorly reconstructed events and to select a region of phase space where the acceptance is well determined and relatively constant as a function of the kinematic variables, the following kinematic cuts were applied to the final sample:

$$\begin{aligned} 1 < Q^2 &< 5 \text{ GeV}^2, \\ 40 < W &< 140 \text{ GeV}, \\ |t| &< 0.5 \text{ GeV}^2. \end{aligned} \tag{2}$$

The cross–section measurements are given in the QED Born approximation for electron interactions. The effects of higher order processes are estimated using the HERACLES 4.4 generator [11, 3] to vary from 1 to 3 % in the different Q^2 and W bins, after applying the cut $\Sigma(E - p_z) > 45$ GeV.[4] A systematic error of 2% on these numbers is obtained by varying the effective Q^2 and W dependences of the $\gamma^* p$ cross–section. The small value of the correction is due to the high $\Sigma(E - p_z)$ cut.

Monte-Carlo simulations

For the total and differential cross–sections of elastic ϱ and ϕ production, most corrections are estimated using the DIFFVM Monte Carlo simulation programs, based on the vector meson dominance model, which permits variation of the Q^2, W and t dependences, as well as the vector meson decay angular distributions [12]. The H1 detector response is simulated in detail, and the events are subjected to the same reconstruction and analysis chain as the data. Examples of the good reproduction of the data by the simulations are shown in Fig 2. For background studies, simulations are also performed of elastic ω production. The relative values of the electroproduction of $\varrho : \omega : \phi$ mesons were taken to be 1:1/9:1/8 in the simulations.

The resolution of the variable measurements, estimated with the simulation, are 1.5 GeV for W, 0.08 GeV^2 for Q^2, 0.037 GeV^2 for t and 0.021 GeV/c^2 for $m_{\pi^+\pi^-}$. The values of the t slopes are little affected by the detector resolution. The scattered positron selection criteria induce Q^2 dependent losses for $Q^2 \leq 2$ GeV^2. The charged track selection criteria induce W dependent losses for high W.

[3] The summation is on all the particles in the final state.

[4] In an ideal event, $\Sigma(E - p_z)$ equals twice the initial positron energy. It is estimated here using the measured vector meson and positron four–momenta.

3 Results

3.1 Mass distribution

Fig. 3a shows the acceptance corrected invariant $\pi^+\pi^-$ mass distribution for the events passing all selection cuts, when the pion mass is assigned to the detected particles in the central tracking detector. The events compatible with $\phi \to K^+K^-$ production ($m_{K^+K^-} < 1.04$ GeV/c^2, when the two charged particles are assigned the kaon mass) have been discarded, and the remaining ω and ϕ background, estimated from the Monte–Carlo simulations, have been substracted statistically. A clear ϱ signal is observed which contains 498 events in the mass region $0.6 < m_{\pi^+\pi^-} < 1.1$ GeV/c^2.

The mass distribution is skewed compared to the Breit-Wigner distribution: an enhancement is observed of the low mass events and a suppression at the high mass side. This asymmetric shape of the distribution is a well known feature of ϱ photoproduction. It has been attributed to an interference between the resonant and non–resonant production of two pions [13]. In order to extract the contribution of the resonant part of the cross-section, the two different procedures, proposed in refs. [14, 15] are used here.

Following the phenomenological parameterisation of Ross and Stodolsky [14], the $m_{\pi^+\pi^-}$ distribution is described as:

$$\frac{dN(m_{\pi\pi})}{dm_{\pi\pi}} = f_\varrho . BW_\varrho(m_{\pi\pi}).(m_\varrho/m_{\pi\pi})^n + f_{bg}, \tag{3}$$

where f_ϱ is a normalisation constant, and

$$BW_\varrho(m_{\pi\pi}) = \frac{m_{\pi\pi}\ m_\rho\ \Gamma(m_{\pi\pi})}{(m_\rho^2 - m_{\pi\pi}^2)^2 + m_\rho^2\ \Gamma^2(m_{\pi\pi})}, \tag{4}$$

is a relativistic Breit-Wigner function with momentum dependent width [16]

$$\Gamma(m_{\pi\pi}) = \Gamma_\rho\ (\frac{q^*}{q_0^*})^3\ \frac{2}{1 + (q^*/q_0^*)^2}. \tag{5}$$

Here, m_ρ and Γ_ρ are the ϱ resonance mass and width, q^* is the pion momentum in the $(\pi^+\pi^-)$ rest frame and q_0^* is this momentum when $m_{\pi^+\pi^-} = m_\rho$. The factor $(m_\varrho/m_{\pi\pi})^n$ in eq. (3) accounts for the skewing of the shape of the ϱ signal. The background term, f_{bg} has been parameterised using a phase space distribution, including a two pion threshold and an exponential fall off:

$$f_{bg} = \alpha_1\ (m_{\pi\pi} - 2m_\pi)^{\alpha_2}\ e^{-\alpha_3 m_{\pi\pi}}, \tag{6}$$

where m_π is the pion mass and α_1, α_2 and α_3 are constants.

With parameterisation (3), the mass distribution was fit over the range $0.3 < m_{\pi^+\pi^-} < 2.0$ GeV/c^2 with the parameters f_ϱ, m_ρ, Γ_ρ, n, α_1, α_2, and α_3 left free. The result is shown in Fig. 3a ($\chi^2/ndf = 28.7/20$). The resonance mass is found to be 783 ± 7 MeV/c^2 and the width 172 ± 16 MeV/c^2, in agreement with the Particle Data Group (PDG) values of 770 and 151 MeV/c^2 [17]. The background contribution is very small under the peak, and corresponds to 2.5 % of the number of events.

The data were also analysed using the parameterisation proposed by Söding, in which the skewing of the mass spectrum is explained by the interference of a resonant $\varrho \to \pi^+\pi^-$ amplitude and a p-wave $\pi\pi$ Drell type background term [15]:

$$\frac{dN(m_{\pi\pi})}{dm_{\pi\pi}} = f_\varrho . BW_\varrho(m_{\pi\pi}) + f_I . I(m_{\pi\pi}) + f_{bg}, \tag{7}$$

$$I(m_{\pi\pi}) = \frac{{m_\rho}^2 - {m_{\pi\pi}}^2}{({m_\rho}^2 - {m_{\pi\pi}}^2)^2 + {m_\rho}^2\Gamma^2(m_{\pi\pi})}, \tag{8}$$

where f_I is a constant, fixing the relative normalisation of the interference contribution. In view of uncertainties on the phase between the resonance and the interference, no constraint is made on the background and interference terms.

The Söding parameterisation also describes the data well in the range $0.55 < m_{\pi^+\pi^-} < 1.1$ GeV/c^2, with values for the resonance mass and width in agreement with the Particle Data Group (PDG) values. The data do not require a significant contribution from non-resonant diffractive background.

The fit procedures, following the Ross–Stodolsky and the Söding parameterisations, were repeated in 3 bins in Q^2, in order to measure the Q^2 dependence of the skewing of the ϱ mass distribution (Fig. 4). In this case, the width and the mass of the ϱ meson were fixed to the PDG values in order to reduce statistical uncertainties, and the fits were performed assuming no background ($f_{bg} = 0$), with 2 free parameters: the overall normalisation and the skewing parameters, n and f_I/f_ϱ respectively. Fig. 5 shows the fit values of the skewing parameters as a function of Q^2. The skewing of the mass distribution is observed to decrease with Q^2. No significant W or t dependence of the skewing was observed within the data.

In Fig. 3b, a clear ϕ signal is observed in the invariant K^+K^- mass distribution, containing 56 events in the range $|m_{K^+K^-} - m_\phi| < 0.02$ GeV/c^2. The superimposed curve is the result of a fit to a relativistic Breit-Wigner distribution (with a width fixed at the PDG value [17]), convoluted with a Gaussian distribution, over a linear background starting at threshold ($m_{KK} = 2\ m_K$). The fited mass of the ϕ meson is 1021.1 ± 1.0 MeV/c^2, in agreement with the PDG value of 1019.4 MeV/c^2. The r.m.s. of the Gaussian distribution, which reflects the detector resolution, is 3.5 ± 1.1 MeV/c^2 in agreement with the value of the Monte–Carlo simulation. The non ϕ background under the signal in the mass region $|m_{K^+K^-} - m_\phi| < 0.02$ GeV/c^2 is estimated to be $15.2 \pm 4.9\%$, where the error includes statistical and systematic uncertainties estimated by varying the shape of the background. Using a Monte-Carlo simulation for ϱ and ω electroproduction, the non ϕ background under the signal was found to be consistent with the reflection of ω and ϱ production, when assigning the kaon mass to the two charged particles.

3.2 ep cross–sections

The cross–sections for elastic production of the ϱ and the ϕ mesons are computed using the events in the mass ranges:

$$0.60 < m_{\pi^+\pi^-} < 1.10 \text{ GeV/c}^2 \quad \text{for the } \varrho, \tag{9}$$

$$1.00 < m_{K^+K^-} < 1.04 \text{ GeV/c}^2 \quad \text{for the } \phi. \tag{10}$$

For ϱ production, the cross-section is computed for the resonant part only, excluding any skewing factor, and a correction is applied for the part of the Breit–Wigner distribution outside the mass range (9) but with $2m_\pi < m_{\pi^+\pi^-} < 1.52$ GeV/c^2. This correction amounts to 17% and 15% using equations (3) and (7) respectively.

In addition to the background mentioned above, a common background to both the ϱ and ϕ production is diffractive vector meson production with proton dissociation. It was determined for the ϱ mesons at high Q^2 to be $9 \pm 8\%$ of the selected signal, using Monte Carlo simulations cross checked directly with the data [3]. The proton dissociation background is assumed to be the same for the present ϱ and ϕ analyses. The uncertainty in the Breit-Wigner form factor [16] amounts to an additioinal error of 2%. In the ϕ case, a correction is applied for the tail of the signal outside the quoted mass range (10).

After corrections for efficiencies and acceptances, for the Breit-Wigner tail, for backgrounds, for QED radiation effects and for the known decay branching ratios of 100% for $\varrho \to \pi^+\pi^-$ and 49% for $\phi \to K^+K^-$, the ep cross–sections for elastic ϱ and ϕ production are:

$$\sigma(ep \to e\varrho p) = 7.04 \pm 0.35 \text{ (stat.)} \pm 0.89 \text{ (syst.) nb}, \tag{11}$$

$$\sigma(ep \to e\phi p) = 1.49 \pm 0.20 \text{ (stat.)} \pm 0.22 \text{ (syst.) nb}, \tag{12}$$

integrated over t and over the range $1 < Q^2 < 5$ GeV^2 and $40 < W < 140$ GeV.

3.3 $\gamma^* p$ cross–section

The ep cross–section is converted into a $\gamma^* p$ cross–section using the relation

$$\frac{\mathrm{d}^2\sigma(ep \to eVp)}{\mathrm{d}y \ \mathrm{d}Q^2} = \Gamma \ \sigma(\gamma^* p \to Vp), = \Gamma \ \sigma_T(\gamma^* p \to Vp) \ (1 + \varepsilon \ R), \tag{13}$$

where ε is the polarisation parameter and $R = \sigma_L/\sigma_T$, is the ratio of longitudinal to transverse $\gamma^* p$ cross sections. Γ is the flux of transverse virtual photons given, for small values of y, by

$$\Gamma \simeq \frac{\alpha \ (1 - y + y^2/2)}{\pi \ y \ Q^2}. \tag{14}$$

The $\gamma^* p$ cross–sections for ϱ and ϕ meson elastic production are presented in the form $(\sigma_T + \sigma_L) \ (\gamma^* p \to Vp)$ as a function of W in Fig. 6, for the quoted average Q^2 values of 2.0 GeV^2 for the ϱ production, and 2.5 GeV^2 for the ϕ production, together with a compilation of photoproduction and leptoproduction results [1, 2, 3, 4, 5, 6]. The statistical and systematic errors are combined quadratically. The measurements from other experiments were scaled, when necessary, to the quoted value of Q^2, using their measured Q^2 dependence and the relevant values of the polarisation parameter ε. Overall normalisation uncertainties quoted by other experiments are not shown. It should be noted that several procedures have been used by the different experiments to correct the $m_{\pi^+\pi^-}$ measurements for the tail of the mass distribution, but they lead to results approximately equivalent to the procedure used here, i.e. for a non–skewed Breit-Wigner distribution, with $2m_\pi < m_{\pi^+\pi^-} < 1.52$ GeV/c^2.

The Q^2 dependence of the $\gamma^* p$ cross–section for elastic ϱ and ϕ production can be described by a form $(Q^2 + m_V^2)^{-n}$ with:

$$n = 1.92 \pm 0.23 \quad \text{for the } \varrho, \tag{15}$$

$$n = 2.34 \pm 0.22 \quad \text{for the } \phi, \tag{16}$$

for a mean W of ≈ 100 GeV. For the ϱ analysis, the fit is performed using only the present measurement. For the ϕ analysis, the data points at higher Q^2 measured by this experiment [4] are fit together with the present measurement.

3.4 t dependence

Fits to the t distributions of the form e^{bt} for $|t| < 0.5$ GeV^2 (Fig. 7) give for the slopes the values:

$$b = 8.0 \pm 0.5 \text{ (stat.) } {}^{+0.7}_{-0.4} \text{ (syst.) GeV}^{-2} \quad \text{for the } \varrho, \tag{17}$$
$$b = 5.6 \pm 1.3 \text{ (stat.)} \pm 0.6 \text{ (syst.) GeV}^{-2} \quad \text{for the } \phi. \tag{18}$$

This result is corrected for the presence of the two sources background mentioned in sections 3.1 and 3.2 with fixed relative contributions with respect to the elastic signal and with fixed slopes, assuming an exponential distribution. The slope of the proton dissociation background is assumed to be $b = 2.5 \pm 1.0$ GeV^{-2}. No dependence of the slope on the proton excitation mass is assumed. The slope for the non-resonant background is taken to be $b = 0.15 \pm 0.1$ GeV^{-2} for the ϱ and $b = 5.9 \pm 1.0$ GeV^{-2} for the ϕ. This value for the ϕ is obtained from the Monte–Carlo simulations as the reflection of the ϱ and ω production, and is compatible with a value measured with the present data for event with $1.04 < m_{K^+K^-} < 1.30$. The systematic errors include the effects of varying within errors the amounts of backgrounds and their b slopes, and of changing the details of the fitting procedure. Fig. 8 shows the t slopes for elastic ϱ and ϕ production in fixed target [2] and HERA [3, 5] experiments as a function of Q^2. Compared with results at low Q^2, a clear decrease with Q^2 of the slope parameters is observed.

3.5 Polarisation

Information on the vector meson production process can be obtained from the angular distributions of the decay particles studied in the vector meson rest frame, the vector meson direction in the $\gamma^* p$ centre-of-mass system being taken as the quantization axis (s–channel helicity system). Three angles are defined: the polar (θ^*) and azimuthal (φ^*) angles of the positive decay particle and the angle ϕ between the vector meson production plane and the electron scattering plane. The decay angular distribution $W(\cos\theta^*, \varphi^*, \phi)$ is related to the spin density matrix elements by the formalism presented in [18]. After integration over the angles φ^* and ϕ, the $W(\cos\theta^*, \varphi^*, \phi)$ distribution becomes

$$\frac{\mathrm{d}N}{\mathrm{d}\cos\theta^*} \propto 1 - r^{04}_{00} + (3\, r^{04}_{00} - 1)\ \cos^2\theta^*. \tag{19}$$

This equation depends only on the density matrix element r^{04}_{00}, which is the probability of finding the vector meson in the helicity state 0 (longitudinal polarisation). Fig. 9a and 9b show the acceptance corrected distributions of $\cos\theta^*$ for the selected ϱ and ϕ samples, after subtraction of the background ($2 \pm 2\%$ of non-resonant background for the ϱ, which is consistent with being flat in $\cos\theta^*$, and $15 \pm 5\%$ of ϱ and ω reflection background for the ϕ, as obtained from the Monte–Carlo simulations). The fit of eq. (19) to the distributions in Fig. 9 gives:

$$r^{04}_{00} = 0.51 \pm 0.04 \pm 0.02 \quad \text{for the } \varrho,$$
$$r^{04}_{00} = 0.32 \pm 0.10 \pm 0.03 \quad \text{for the } \phi. \tag{20}$$

The first error is statistical, the second reflects the uncertainty on the background subtraction and the fit procedure.

The s–channel helicity conservation (SCHC) hypothesis states that the helicity of the virtual photon is retained by the ϱ meson. In this case, r^{04}_{00} is related to R, the ratio of the longitudinal to transverse cross–sections:

$$R = \frac{1}{\varepsilon}\ \frac{r^{04}_{00}}{1 - r^{04}_{00}}. \tag{21}$$

With the asssumption of SCHC, the cross–section ratio is found to be

$$R = \sigma_L/\sigma_T\ (\gamma^* p \to \varrho p) = 1.03\ {}^{+0.17}_{-0.15}\ {}^{+0.09}_{-0.08} \quad \text{for the } \varrho, \tag{22}$$

$$R = \sigma_L/\sigma_T\ (\gamma^* p \to \phi p) = 0.47\ {}^{+0.26}_{-0.19}\ {}^{+0.07}_{-0.06} \quad \text{for the } \phi. \tag{23}$$

The value of R for ϱ production is shown as a function of Q^2, in Fig. 10 together with HERA data [3, 5] and fixed target measurements [2].

In case of ϱ production, a further study was performed of the polarisation angles. Under the SCHC assumption, the angular distribution $W(\cos\theta^*, \varphi^*, \phi)$ reduces to $W(\cos\theta^*, \psi)$, where $\psi = \phi - \varphi^*$ is the angle between the ϱ decay plane and the lepton scattering plane. In spite of an important smearing on the angles ϕ and φ^*, the strong correlation between them allows the measurement of ψ with a good accuracy. If in addition the exchange in the t-channel is assumed to have natural spin–parity, then $W(\cos\theta^*, \psi)$ takes the following form:

$$W(\cos\theta^*, \psi) = \frac{3}{8\pi}\ \frac{1}{1+\varepsilon\ R}\ \{\ \sin^2\theta^*\ [1+\varepsilon\ \cos(2\psi)\ ]$$
$$+\ 2\ \varepsilon\ R\ \cos^2\theta^*\ -\sqrt{2\ \varepsilon\ (1+\varepsilon)\ R}\ \cos\delta\ \sin(2\theta^*)\ \cos\psi\ \}, \tag{24}$$

where δ is the phase angle between the amplitudes for longitudinal and transverse ϱ production, a value $\cos\delta$=1 indicating that both amplitudes are in phase. The effect of this interference can be seen on the scatter plot ($\cos\theta^*$, ψ) in Fig. 11a. A two dimensional fit using eq (24) gives for $\cos\delta$ and R parameter the values:

$$\cos\delta = 0.88 \pm 0.04\ (stat.) \pm 0.05\ (syst.), \tag{25}$$

$$R = 1.27 \pm 0.18. \tag{26}$$

The systematic error includes uncertainty on the Monte–Carlo simulations. The value obtained for R (statistical error only) is in agreement with that optained from the ψ integrated angular distribution $W(\cos\theta^*)$ in eqs. (19) and (21). Fig. 11b shows the $\cos\delta$ parameter for elastic ϱ production, together with fixed target [2] experiments, as a function of Q^2.

4 Cross section ratio $\sigma(\phi)/\sigma(\varrho)$

For the measurement of the ratio of the cross–sections for elastic electroproduction of ϕ and ϱ mesons, the same selection criteria are used for both data samples, in order to minimise the systematic effects. These largely cancel in the ratio, except for a small difference in the acceptances for the two samples, due to the different opening angles between the two decay hadrons in the laboratory frame, which is taken into account.

After acceptance correction and background subtraction from the two samples, the ϕ to ϱ cross–section ratio $R_{\phi/\varrho}$ is measured to be:

$$R_{\phi/\varrho} = 0.132 \pm 0.027 \pm 0.004 \qquad \text{for } Q^2 = 1.3\ \text{GeV}^2, \tag{27}$$

$$R_{\phi/\varrho} = 0.155 \pm 0.030 \pm 0.005 \qquad \text{for } Q^2 = 2.6\ \text{GeV}^2, \tag{28}$$

for $W \approx 80$ GeV. These results are presented in Fig. 12 together with values from photoproduction data [1] and high Q^2 data [4, 6]. The present result confirms the significant rise of the cross–section ratio with Q^2. The result for two bins in W is:

$$R_{\phi/\varrho} = 0.136 \pm 0.028 \pm 0.004 \qquad \text{for } W = 58\ \text{GeV}, \tag{29}$$

$$R_{\phi/\varrho} = 0.145 \pm 0.028 \pm 0.004 \qquad \text{for } W = 102\ \text{GeV}, \tag{30}$$

for $Q^2 \approx 2$ GeV^2. Within errors, no dependence on W is observed.

5 Conclusion

The cross–section for elastic electroproduction of ϱ and ϕ mesons has been measured at HERA, for $1 < Q^2 < 5$ GeV^2 and $40 < W < 140$ GeV. The Q^2 dependence of the $\gamma^* p \ \rightarrow Vp$ cross–section is well described in the present data by the form $(Q^2 + m_V)^{-n}$ with $n = 1.92 \pm 0.23$ for the ϱ meson and, using high Q^2 measurements, $n = 2.34 \pm 0.22$, for the ϕ meson. The t distributions are parameterised as exponentially falling, with a slope $b = 8.0 \pm 0.5 \ ^{+0.7}_{-0.4}$ GeV^{-2} for the ϱ and $b = 5.7 \pm 1.3 \pm 0.6$ GeV^{-2} for the ϕ. Assuming SCHC, the longitudinal to transverse cross–section ratio for virtual photons is measured to be $R = 1.03 \ ^{+0.17}_{-0.15} \ ^{+0.09}_{-0.08}$ for the ϱ and $R = 0.47 \ ^{+0.26}_{-0.19} \ ^{+0.07}_{-0.06}$ for the ϕ. For the ϱ, the $\cos\delta$ phase between longitudinal and transverse ϱ production is $0.88 \pm 0.04 \pm 0.05$. Finally, the ratio of the cross–sections for elastic electroproduction of ϕ and ϱ mesons is determined to be $R_{\phi/\varrho} = 0.132 \pm 0.027 \pm 0.004$ for $Q^2 = 1.3$ GeV^2, and $R_{\phi/\varrho} = 0.155 \pm 0.030 \pm 0.005$ for $Q^2 = 2.6$ GeV^2.

Acknowledgements

We are grateful to the HERA machine group whose outstanding efforts have made and continue to make this experiment possible. We thank the engineers and technicians for their work in constructing and now maintaining the H1 detector, our funding agencies for financial support, the DESY technical staff for continual assistance, and the DESY directorate for the hospitality which they extend to the non-DESY members of the collaboration. We thank further E. Gallo, H. Beier, T. Monteiro for providing us with preliminary ZEUS results.

References

[1] a. S. Aid et al., H1 Coll., *Nucl. Phys.* **B463** (1996) 3;
b. M. Derrick et al., ZEUS Coll., *Zeit. Phys.* **C69** (1995) 39;
c. M. Derrick et al., ZEUS Coll., *Phys. Lett.* **B377** (1996) 259;
d. M. Derrick et al., ZEUS Coll., *Zeit. Phys.* **C73** (1997) 253;
e. ZEUS Coll., Contributed paper to the XXVIIIth International Conference on High Energy Physics, Warsaw, July 1996, Ref. pa-02-050.

[2] a. J.T. Dakin et al., *Phys. Rev. Lett.* **30** (1973) 142;
b. V. Eckardt et al., *Nucl. Phys.* **B55** (1973) 45;
c. C. del Papa et al., *Phys. Rev.* **D19** (1979) 1303;
d. D.G. Cassel et al., *Phys. Rev.* **D24** (1981) 2787;
e. W.D. Shambroom et al., CHIO Coll., *Phys. Rev.* **D26** (1982) 1;
f. M. Arneodo et al., NMC Coll., *Nucl. Phys.* **B429** (1994) 503;
g. M.R. Adams et al.,E665 Coll., *Zeit. Phys.* **C74** (1997) 237.

[3] S. Aid et al., H1 Coll., *Nucl. Phys.* **B468** (1996) 3.

[4] S. Aid et al., H1 Coll., "Proton Dissociative ϱ and Elastic ϕ Electroproduction at HERA", DESY-97-082, submitted to Z. Phys. C.

[5] a. M. Derrick et al., ZEUS Coll., *Phys. Lett.* **B356** (1995) 601;
b. ZEUS Coll., Contributed paper to the XXVIIIth International Conference on High Energy Physics, Warsaw, July 1996, Ref. pa-02-028;
c. ZEUS Coll., Contributed paper to the Vth international workshop on deep inelastic scattering and QCD (DIS 97), Chicago, April 1997.

[6] M. Derrick et al., ZEUS Coll., *Phys. Lett.* **B380** (1996) 220.

[7] I. Abt et al., H1 Coll., *Nucl. Instr. Meth.* **A386** (1997) 310;348

[8] H1 SPACAL group, R. D. Appuhn et al., DESY preprint 96-171, submitted to Nucl. Instr. and Meth.

[9] T. Ahmed et al., H1 Coll., *Phys. Lett.* **B348** (1995) 681.

[10] S. Bentvelsen, J. Engelen and P. Kooijman, *Reconstruction of (x, Q^2) and extraction of structure functions in neutral current scattering at HERA,* in: Proc. of the Workshop on Physics at HERA, ed. W. Buchmüller and G. Ingelman, Hamburg 1992, Vol. 1, p. 23;
K.C. Hoeger, *Measurement of x, y, Q^2 in Neutral Current Events,* ibid., p. 43.

[11] H. Spiesberger, *HERACLES 4.4,* unpublished program manual (1993);
A. Kwiatkowski, H. Spiesberger and H.-J. Möhring, *An event generator for ep interactions at HERA including radiative processes,* in: Proc. of the Workshop on Physics at HERA, ed. W. Buchmüller and G. Ingelman, Hamburg 1992, Vol. 3, p. 1294.

[12] *DIFFVM program,* see: B. List, *Diploma Thesis*, Techn. Univ. Berlin, unpubl. (1993).

[13] S.D. Drell, *Phys. Rev. Lett.* **5** (1960) 278.

[14] R. Ross and V. Stodolsky, *Phys. Rev.* **149** (1966) 1173.

[15] P. Söding, *Phys. Lett.* **19** (1966) 702.

[16] T.J. Jackson, *Nuovo Cim.* **34** (1964) 1644.

[17] R.M. Barnett et al., *Review of Particle Properties, Phys. Rev.* **D54** (1996) 1.

[18] K. Schilling and G. Wolf, *Nucl. Phys.* **B61** (1973) 381.

Figures

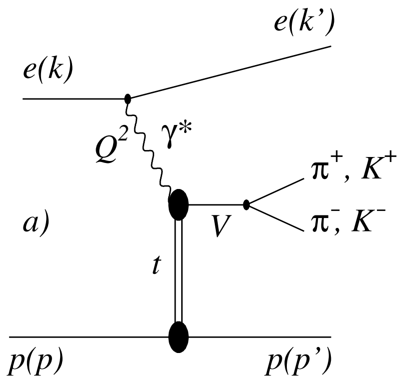

(a)

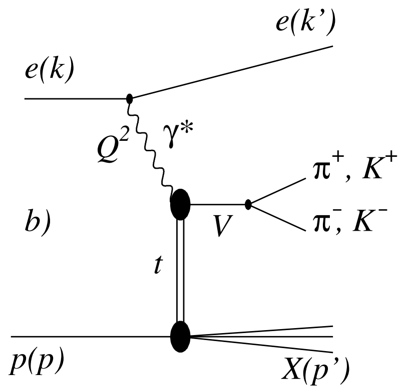

(b)

Figure 1: Electroproduction of ϱ and ϕ mesons: a) elastic process; b) proton dissociation process.

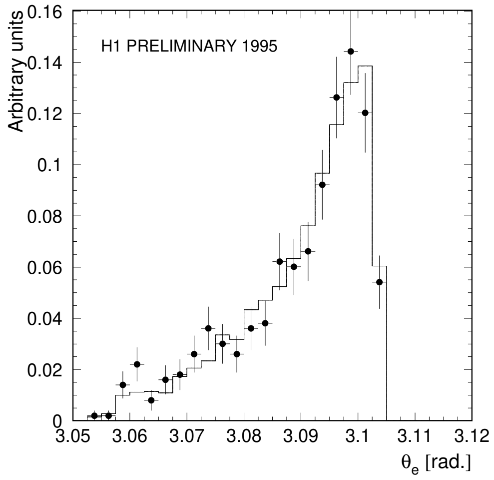

(a)

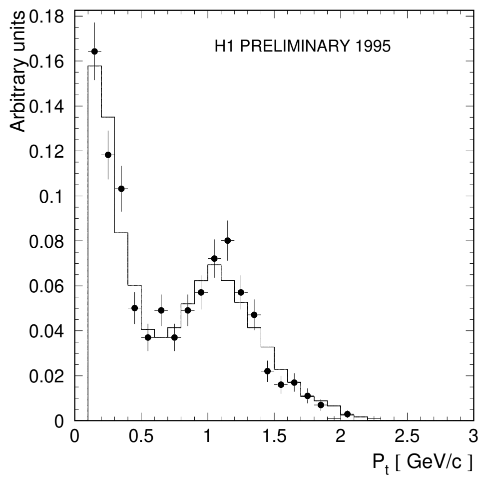

(b)

Figure 2: Distributions of a) the angle of the scattered positron and b) the transverse momenta of the tracks, for the ϱ data (points) and for the Monte–Carlo simulation (histogram).

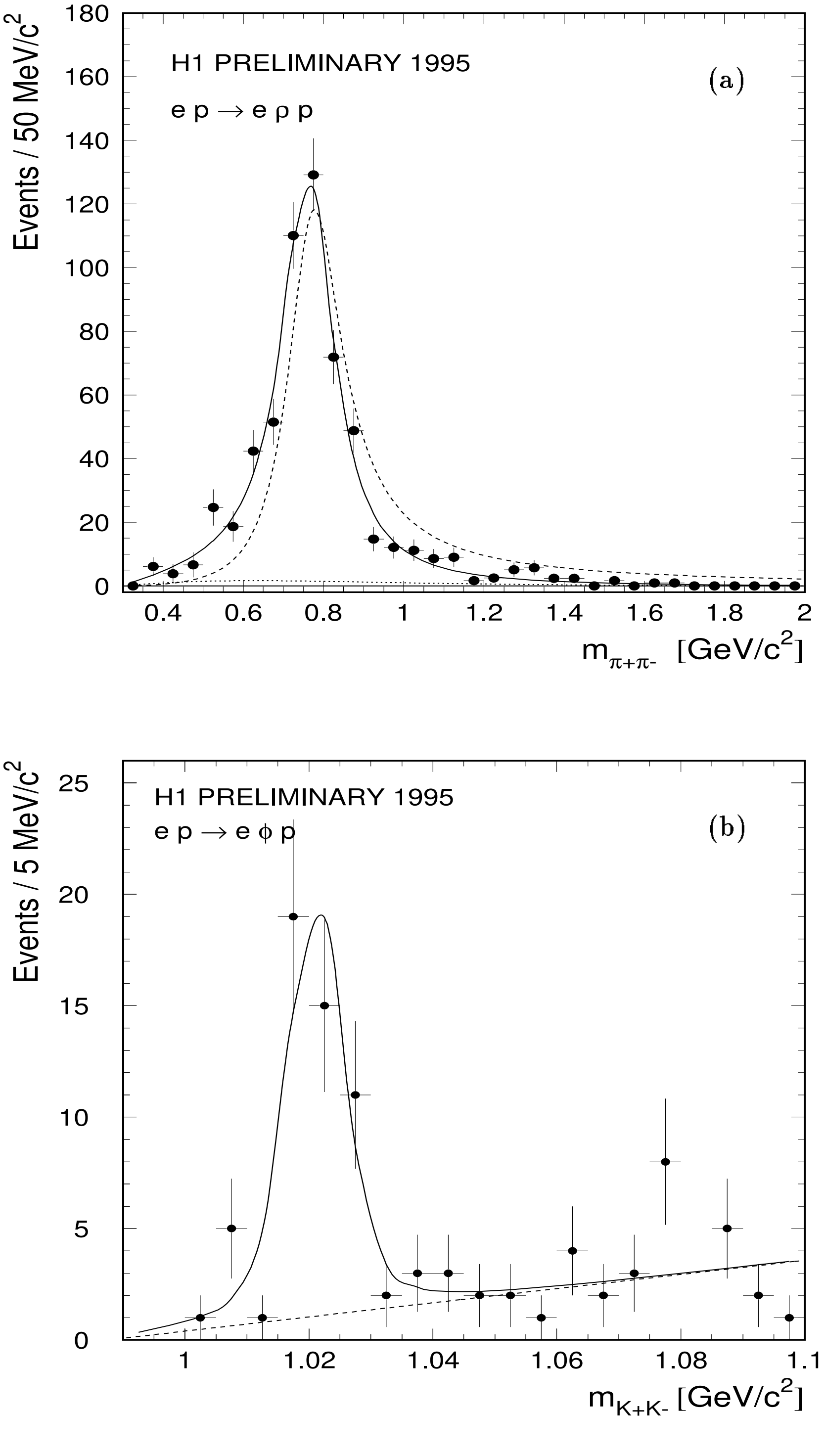

Figure 3: a) Acceptance corrected $m_{\pi^+\pi^-}$ mass distribution for the selected events in the kinematical region specified in the text, with $m_{K^+K^-} > 1.04$, and after statistical substraction of the remaining ω and ϕ backgrounds. The superimposed curve is the result of a fit to a skewed relativistic Breit-Wigner distribution (Ross-Stodolsky parameterisation), over a phase space background (dotted line). The dashed line represents the corresponding non-skewed Breit-Wigner distribution; b) $m_{K^+K^-}$ invariant mass distribution for the selected events eq. (2). The curve is the result of a fit to a relativistic Breit-Wigner distribution convoluted with a Gaussian, over a linear background.

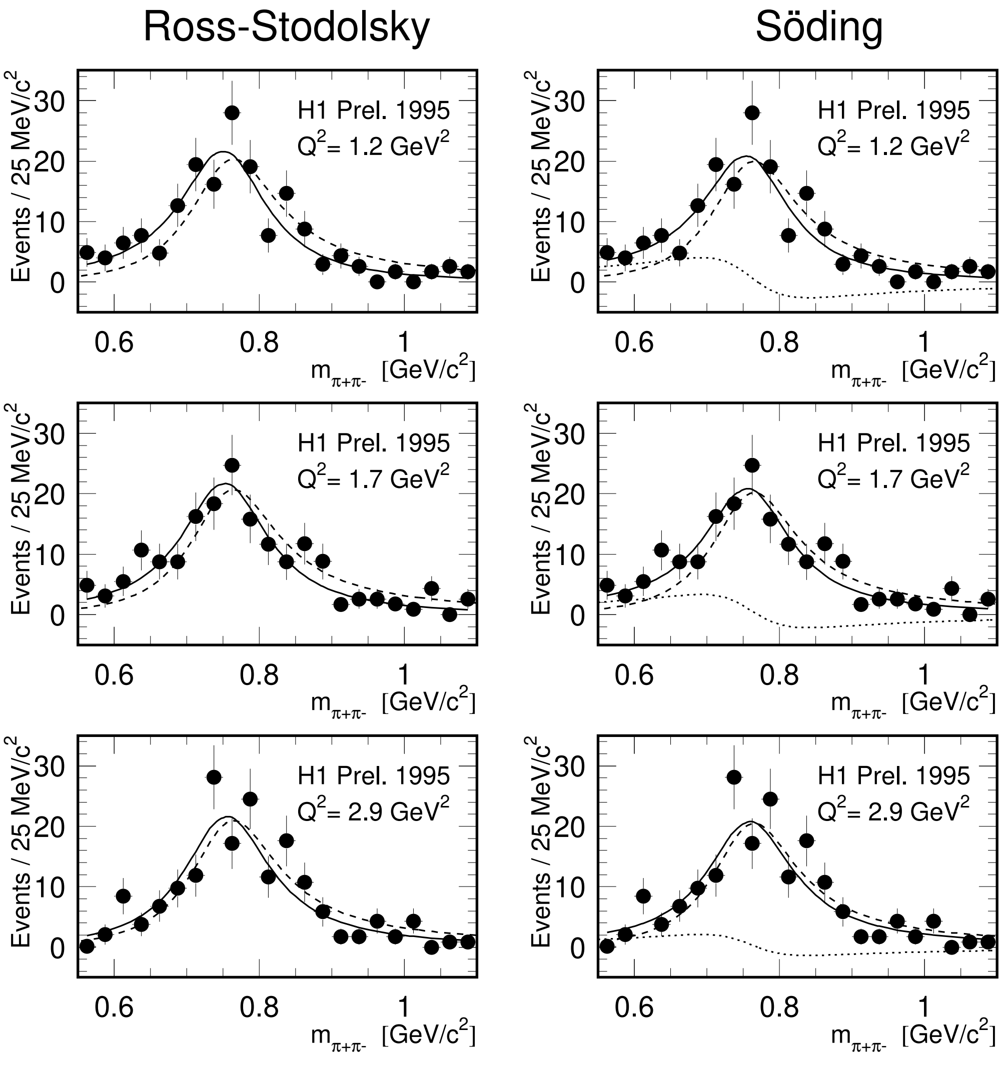

(a) (b)

Figure 4: Acceptance corrected $m_{\pi^+\pi^-}$ mass distribution for the final event sample in three Q^2 bins (low Q^2 at the top, high Q^2 at the bottom) using a) the Ross-Stodolsky parameterisation of eq. (3); b) the Söding parameterisation of eq. (7). The solid line is the result of the fit, the dashed line corresponds to a non-skewed Breit-Wigner contribution. For the Söding parameterisation, the dotted line corresponds to the interference between the resonant and the non–resonant amplitude.

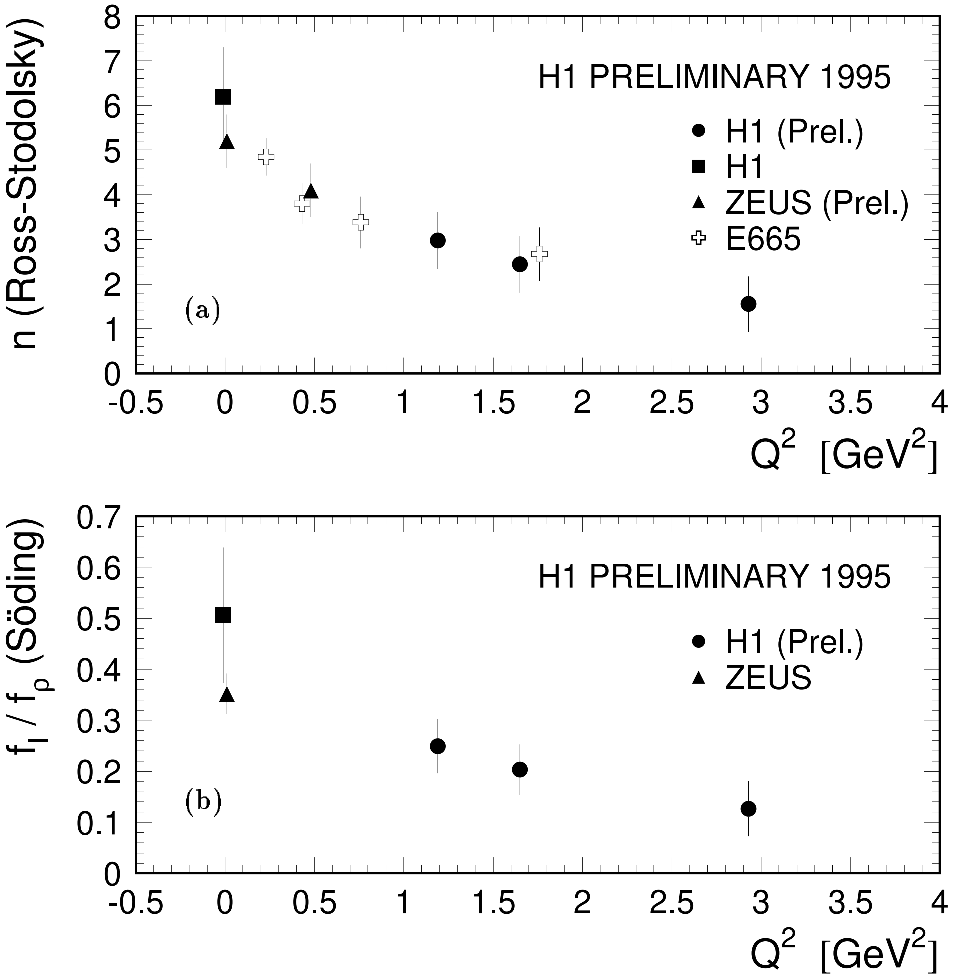

Figure 5: Q^2 dependence of the skewing parameter for elastic ϱ production: a) n, for the Ross-Stodolsky parameterisation of eq. (3); b) f_I/f_ϱ, for the Söding parameterisation of eq. (7).

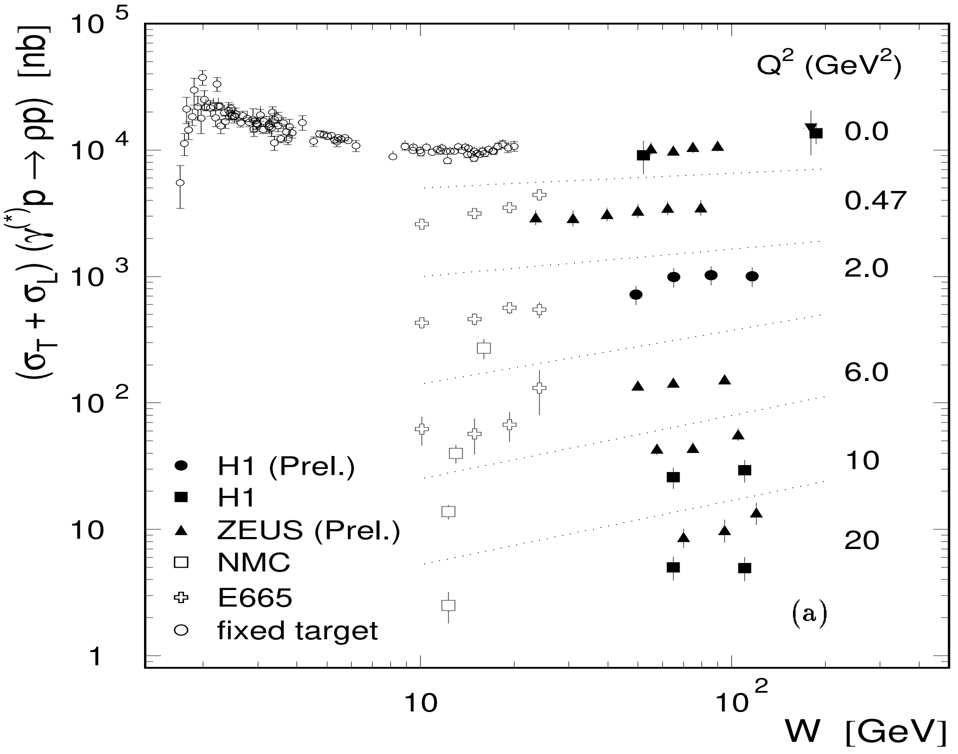

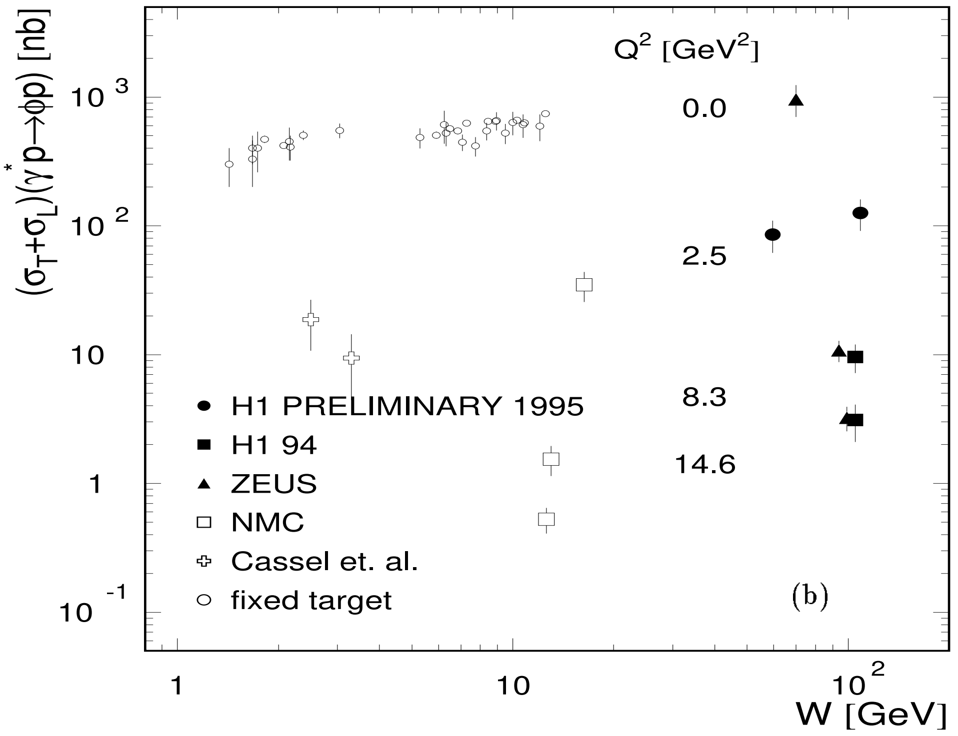

Figure 6: The cross–section $(\sigma_T + \sigma_L)$ $(\gamma^* p \to Vp)$, where σ_T and σ_L are respectively the transverse and longitudinal virtual photon cross–sections, as a function of W a) for ϱ (the dashed lines delimit the different Q^2 domains); b) for ϕ meson production.

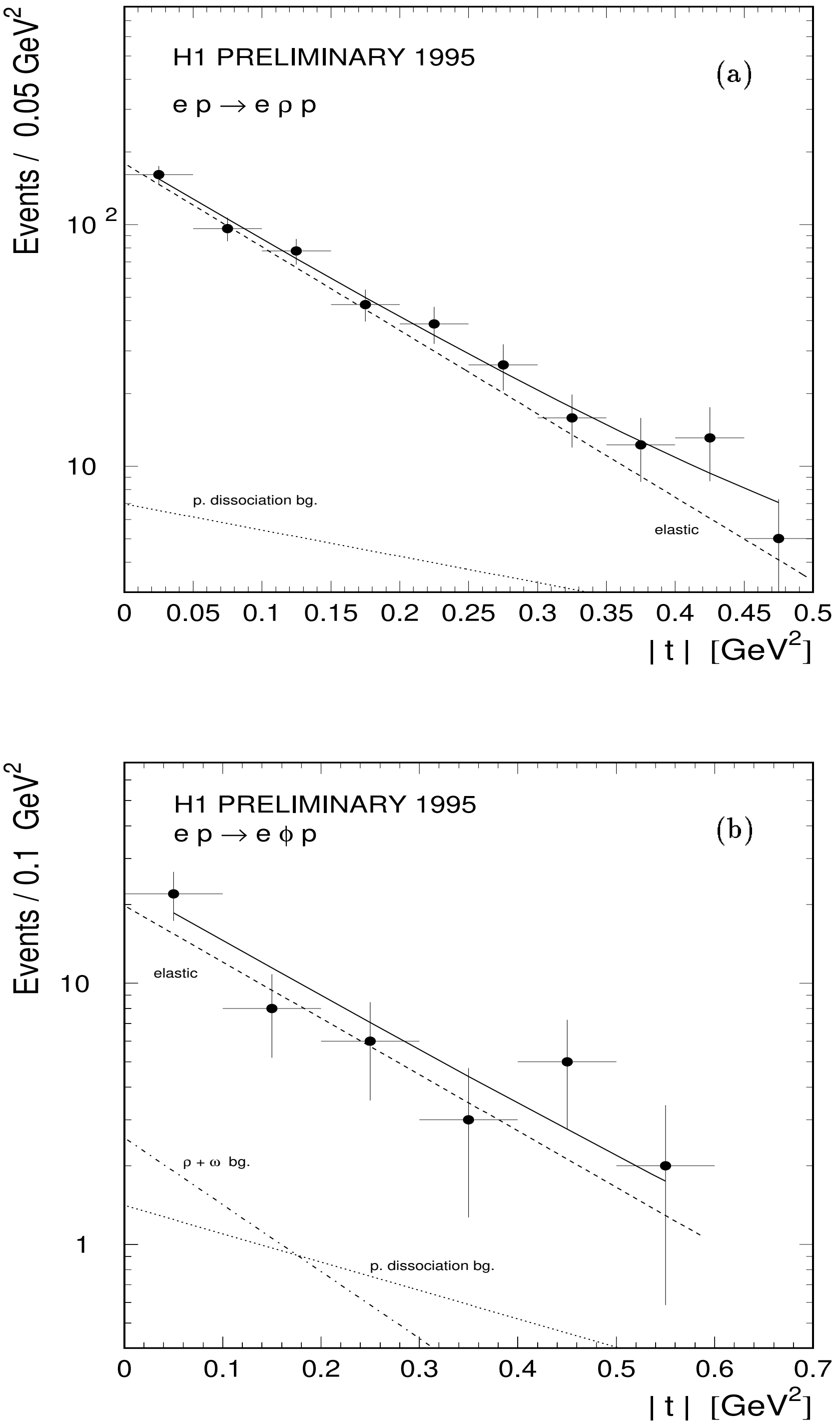

Figure 7: Acceptance corrected t distribution a) for ϱ; b) for ϕ meson production. The full line corresponds to the global fit as a sum of three exponentials, corresponding to the elastic resonant signal, the proton dissociation background and the non–resonant background. The dashed line corresponds to the elastic signal alone, the dotted line to the proton dissociation background, and, in the ϕ case, the dashed dotted line corresponds to the non–ϕ background under the ϕ signal.

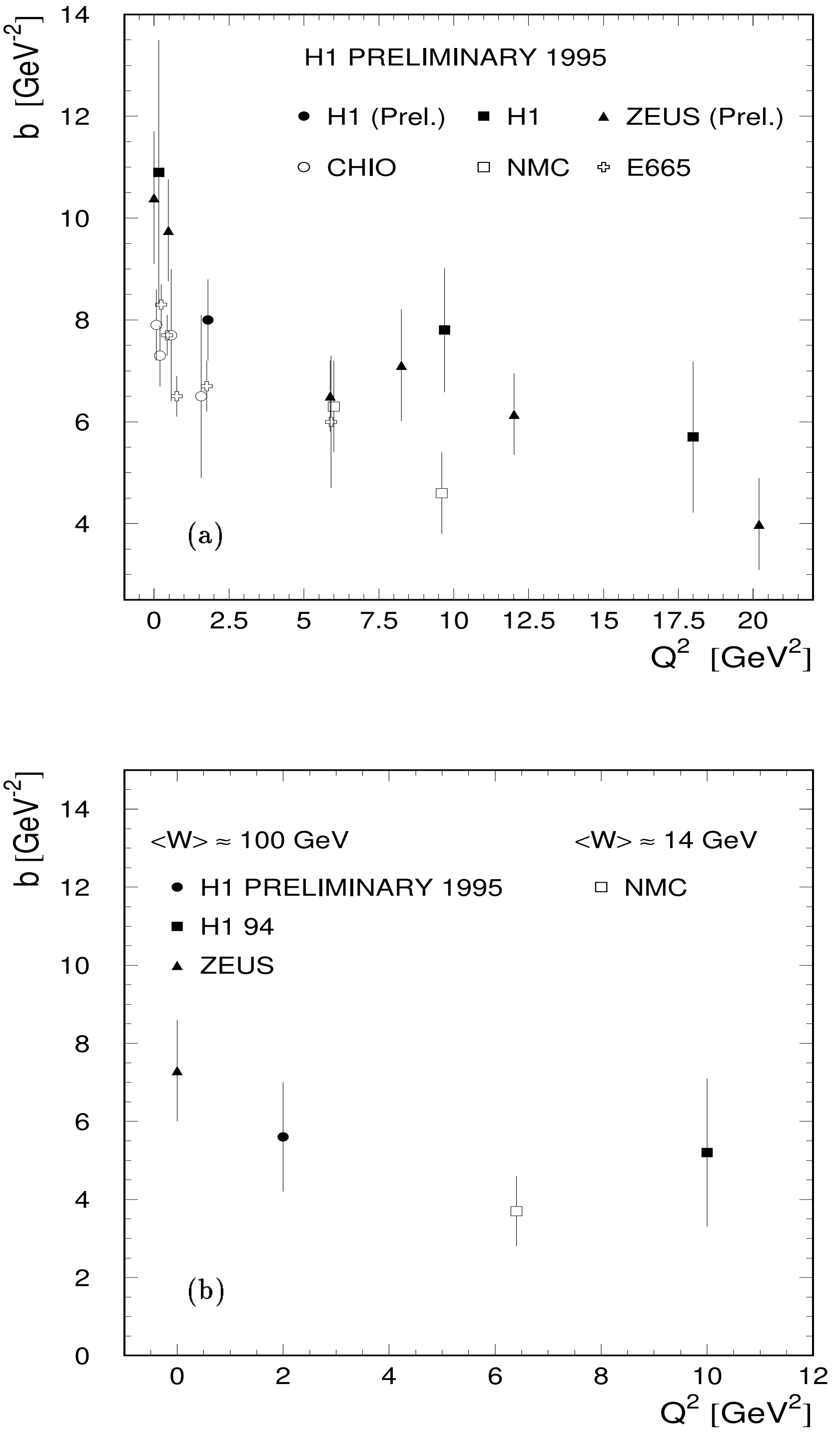

Figure 8: Slope parameter b of the exponentially falling t distribution for elastic a) ϱ, b) ϕ meson production, as a function of Q^2.

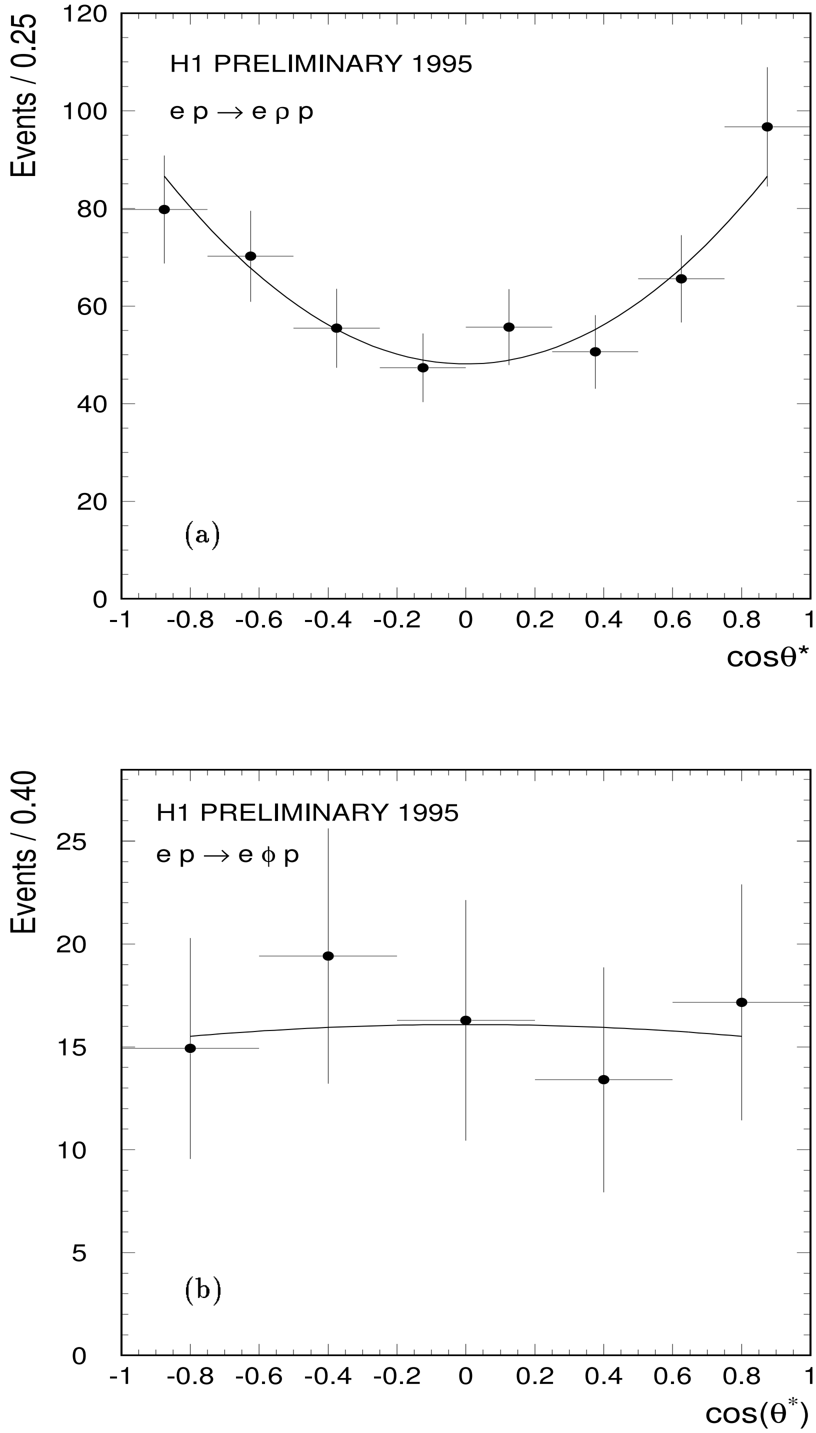

Figure 9: Acceptance and background corrected $\cos\theta^*$ distribution a) for ϱ; b) for ϕ meson production. The superimposed curve is the result of a fit to eq. (19).

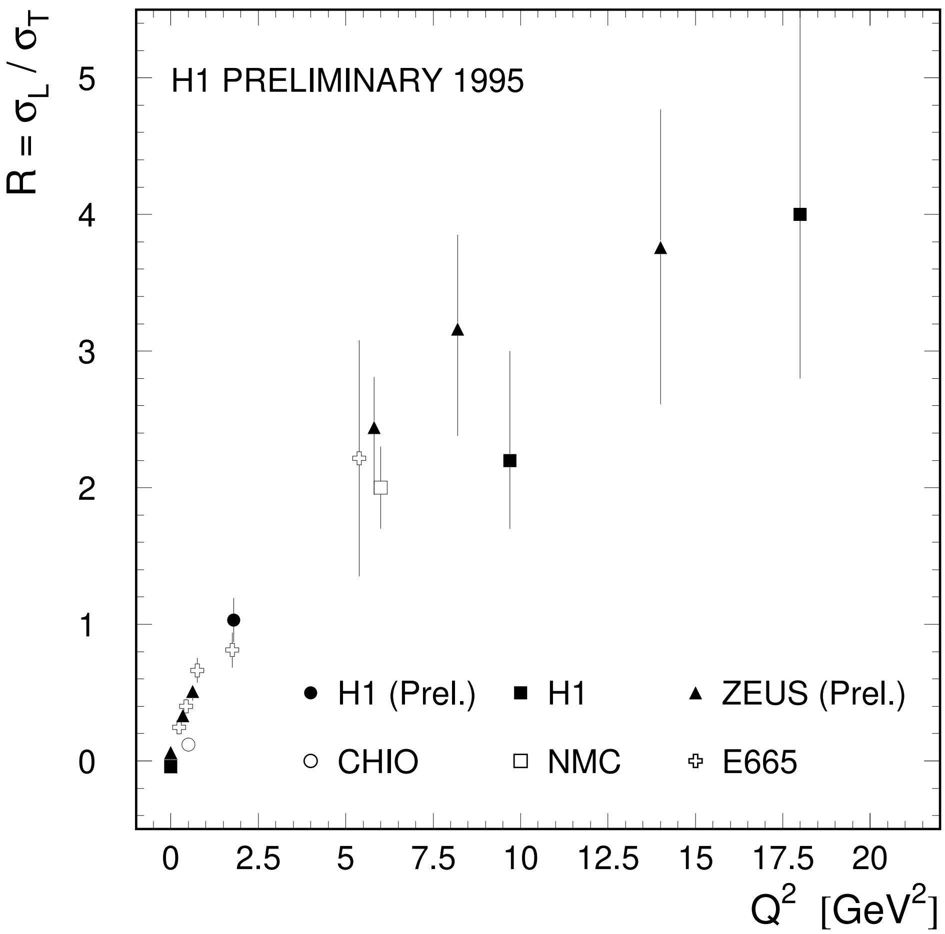

Figure 10: For elastic ϱ meson production, measurement of the ratio of the longitudinal to transverse photon cross–sections as a function of Q^2.

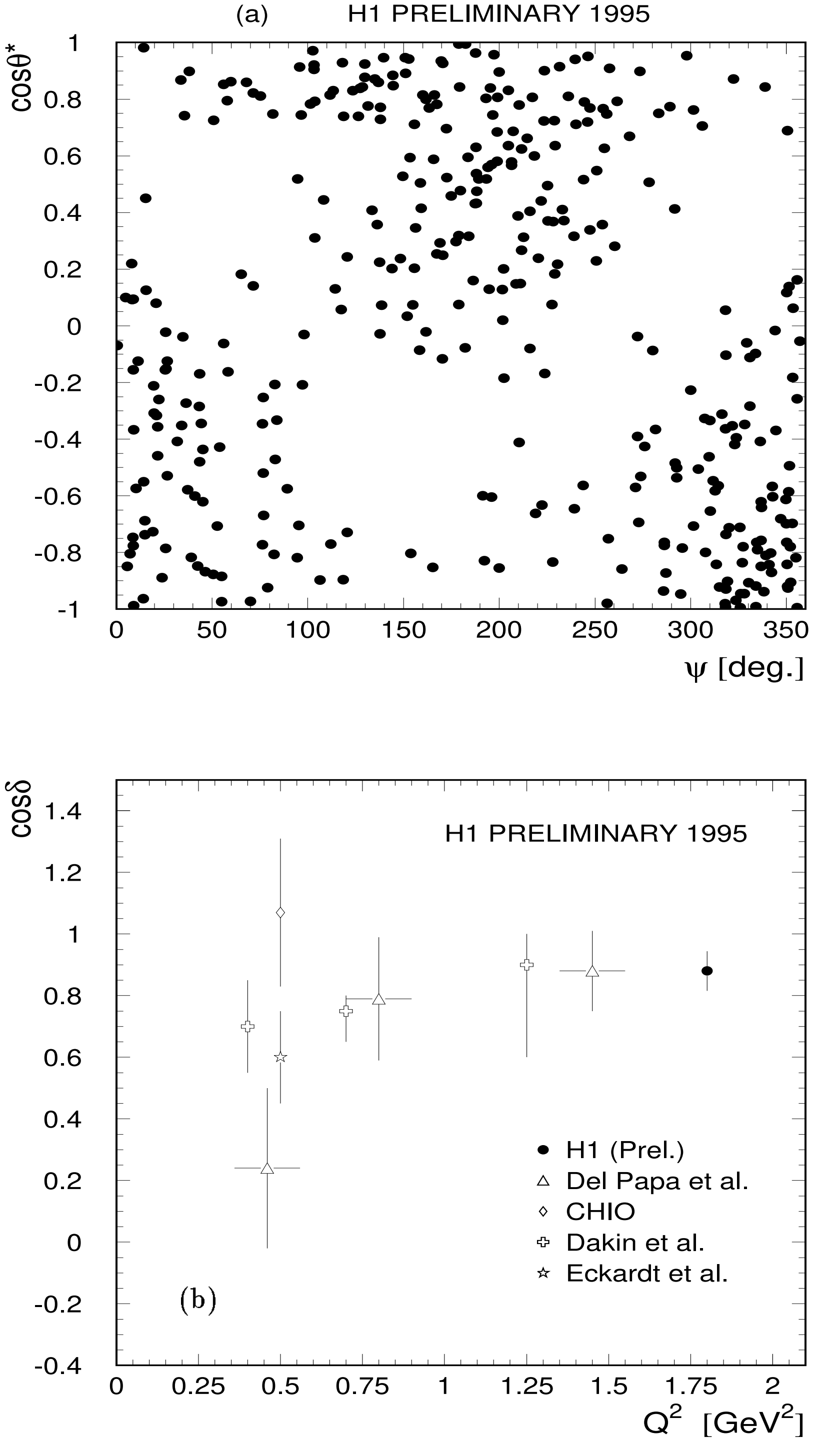

Figure 11: For elastic ϱ meson production: a) acceptance corrected distribution of $\cos\theta^*$ as a function of ψ; b) measurement of the $\cos\delta$ parameter as a function of Q^2 (for $W > 2.5$ GeV).

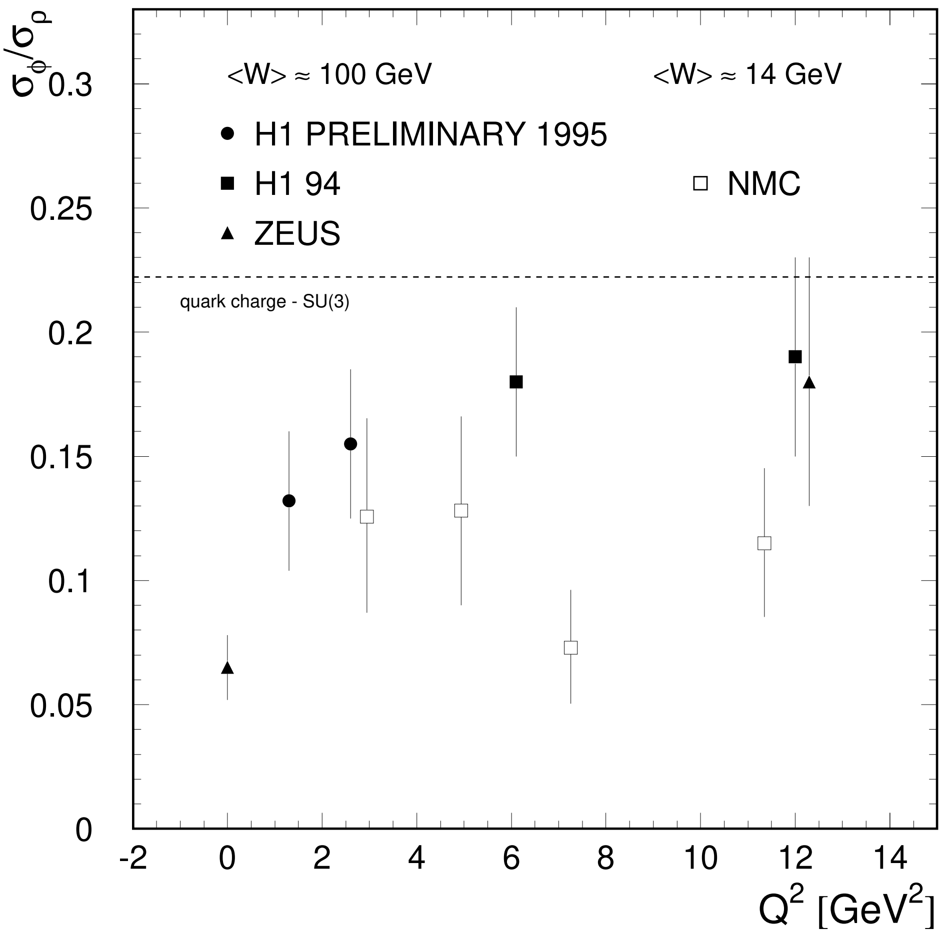

Figure 12: Ratio of the cross–sections for elastic electroproduction of ϕ and ϱ mesons, as a function of Q^2. The horizontal line shows the expectation from quark charge counting, neglecting effects related to the different wave functions of the vector mesons.